VII International Conference on Computational Methods for Coupled Problems in Science and Engineering
COUPLED PROBLEMS 2017
M. Papadrakakis, E. Oñate and B. Schrefler (Eds)

MESHLESS MODELLING OF MICROSTRUCTURE EVOLUTION IN THE CONTINUOUS CASTING OF STEEL

TADEJ DOBRAVEC[*], BOŠTJAN MAVRIČ[*], ROBERT VERTNIK[*,†] AND BOŽIDAR ŠARLER[*,††]

[*] Laboratory for Simulation of Materials and Processes
Institute of Metals and Technology
Lepi pot 11, SI-1000 Ljubljana, Slovenia
e-mail: tadej.dobravec@imt.si, web page: http://www.imt.si

[†] Quality and Development
Štore Steel, d.o.o.
Železarska 3, SI-3220 Štore, Slovenia
e-mail: robert.vertnik@imt.si, web page: http://www.store-steel.si

[††] Laboratory for Fluid Dynamics and Thermodynamics
Faculty of Mechanical Engineering, University of Ljubljana
Aškerčeva 6, SI-1000 Ljubljana, Slovenia
e-mail: bozidar.sarler@fs.uni-lj.si, web page: https://www.fs.uni-lj.si

Key words: Continuous Casting, Steel, Microstructure Evolution, Slice Model, Two-Scale Model, Meshless Methods.

Abstract. A two-dimensional two-scale slice model has been developed to predict the microstructure evolution in the solidifying strand with an arbitrary cross section geometry during continuous casting of steel. The enthalpy equation is solved at the macro level by using meshless local radial basis function collocation method (LRBFCM) based on multiquadrics for spatial discretization and explicit Euler scheme for temporal discretization. The temperature and the solid fraction in computational nodes are calculated by using a continuum model formulation while the lever rule is used as the supplementary microsegregation relation. The temperature field is interpolated to the micro level by using LRBFCM. At the micro level, the normal distribution and Kurz-Giovanola-Trivedi model are proposed to determine temperature dependent nucleation rate and grain growth velocity, respectively. Meshless point-automata algorithm is applied to implement nucleation and grain growth equations. Several examples of computations of the strand with different cross-sections are shown.

1 INTRODUCTION

The continuous casting (CC) is the most widely used technique in the mass steel production since its introduction in the 1950s [1]. The numerical models for simulation of CC of steel represent powerful tools for in-depth understanding and optimization of the casting

process [2, 3]. The development of the numerical models is a very challenging process due to a highly complex nature of the coupled physical phenomena such as fluid flow, heat, mass and solute transport of solidification. These phenomena affect microstructure evolution, having a decisive impact on the material properties of the final product.

The comprehensive three-dimensional numerical models are time consuming, hence alternative approaches are derived for simulation of solidification in the CC. One of the most popular alternative approaches is the so called slice model approximation, where the three-dimensional strand is approximated by a traveling two-dimensional Lagrangian slice, moving with casting velocity in the axial direction. Such simplification is justified, since the conduction is less important than the advection in the axial direction [4]. The constant velocity in the strand has only z-coordinate in this approximation, hence the fluid flow could not be simulated, however the solidification phenomena can still be observed due to the heat and solute transfer in the radial direction [5]. The numerical models for the heat and solute transfer are coupled to the models for the simulation of the microstructure evolution, i.e., nucleation and grain growth. Since the simulation of the microstructure evolution is required on a micrometer scale, the simple grain growth algorithms like the Cellular Automata (CA) [6, 7] are more suitable than the time consuming algorithms like the Phase Field [8, 9, 10]. CA was first used in the CAFE [11] model for the simulation of the nucleation and grain growth along with finite element method that was used to determine the temperature field. A similar approach was used in the two-scale model [12] as the Local Radial Basis Function Collocation Method (LRBFCM) [2] was used for the simulation of the heat transport at the macro level and CA for the nucleation and grain growth at the micro level.

In the present paper, two-scale slice model for the simulation of the microstructure evolution in the continuous casting of steel is presented. Similarly as in the model from [12], the LRBFCM is used for simulation of the temperature field evolution at the macro level. At the micro level, the Point Automata (PA) [13] is used instead of CA, since PA reduces the anisotropy caused by the mesh [14]. The main novelity of this paper is a computationally effective simulation of the microstructure evolution in the continuous casting of steel with arbitrary cross section geometry of the strand. The results of the simulations provide useful qualitative information about the microstructure evolution to engineers in the steel production companies; for example, the dependence of the positions of Equiaxed to Columnar Transitions (ECT) and Columnar to Equaixed Transitions (CET) [4] on the caster geometry and the process parameters.

2 GOVERNING EQUATIONS

The two-scale model describes the heat transfer and the solidification at the macro level and the nucleation and the grain growth at the micro level. The equations are at both scales solved in a transverse Lagrangian slice moving in the axial direction with the casting speed v_{cast}. The temperature field in each slice depends only on its history and on the axial z-coordinate dependent boundary conditions that are determined by the caster geometry and the process parameters. The axial z-coordinate of the slice is determined as

$$z(t) = \int_{t_{start}}^{t} v_{cast}(t')dt' + z_{start}, \tag{1}$$

where t_{start} and z_{start} stand for the initial time and the initial axial coordinate of the slice, respectively.

2.1 Macroscopic model

The heat transfer is described by the heat diffusion equation

$$\frac{\partial(\rho h)}{\partial t} = \nabla \cdot (k \nabla T), \tag{2}$$

where ρ, h, k and T stand for density, enthalpy, thermal conductivity and temperature, respectively. Robin boundary condition is incorporated

$$-k \frac{\partial T}{\partial \hat{n}} = h_0 (T - T_0), \tag{3}$$

where $\hat{n}$, h_0 and T_0 stand for the unit normal vector on the boundary, the effective heat transfer coefficient and the effective surrounding temperature, respectively. The initial temperature in the domain is set to the supercooling ΔT_0 above the liquidus temperature. A linearized eutectic phase diagram is proposed, hence the liquidus and the solidus temperatures T_{liq} and T_{sol} are calculated as

$$T_{liq} = T_m + mC_0, \qquad T_{sol} = T_m + mC_0 / k_p \tag{4}$$

where m, C_0 and k_p stand for the liquidus slope, the concentration of the carbon and the partition coefficient, respectively. The mixture formulation [15] is used to define the enthalpy and the thermal conductivity in the computational domain, containing liquid and solid phase

$$h = f_\ell (c_\ell T + h_\ell^0) + f_s c_s T, \qquad h_\ell^0 = (c_s - c_\ell) T_{sol} + h_f, \tag{5}$$

where f and c stand for mass fraction and specific heat, respectively. The subscripts s and ℓ denote solid and liquid phase. h_f stands for the latent heat of the phase change. The mixture thermal conductivity is defined as

$$k = f_s k_s + f_\ell k_\ell, \tag{6}$$

where k_s and k_ℓ stand for the conductivities in the solid and the liquid phase, respectively. In the present paper the lever rule [4] is used as the supplementary microsegregation relation needed to calculate the enthalpy inverse $T=T(h)$. The use of the lever rule yields the following relation between the solid fraction and the temperature

$$f_s = \frac{1}{1 - k_p} \left[\frac{T - T_{liq}}{T - T_m} \right], \tag{7}$$

where T_m stands for the melting temperature of pure iron.

2.2 Microscopic model

Microscopic model describes nucleation and grain growth as a function of the temperature calculated at the macro level. The nucleation density change dn, induced by the change of the

undercooling $d\Delta T$ is described by the normal distribution

$$\frac{dn}{d\Delta T} = \frac{n_{\max}}{\sqrt{2\pi}\Delta T_\sigma} \exp\left[-\frac{1}{2}\left(\frac{\Delta T - \Delta T_\mu}{\Delta T_\sigma} \right)^2 \right]; \qquad \Delta T = T_{liq} - T, \tag{8}$$

where n_{max}, ΔT_σ and ΔT_μ stand for the maximal nucleation density, the standard deviation and the mean of the undercooling, respectively. Grain growth is in analytical studies described as a growth of a paraboloid with a tip radius R_{tip} and velocity V [4]. In the present model, the Kurz-Giovanola-Trivedi (KGT) model [16] is proposed to determine the relation $V(\Delta T)$. The KGT model consists of two non-linear equations which relate the material properites, C_0, ΔT, V and R_{tip}. In the KGT equations, the non-dimensional Péclet number Pe is introduced

$$\mathrm{Pe} = \frac{R_{tip} V}{2 D_\ell}, \tag{9}$$

where D_ℓ is the solutal diffusion coefficient in the liquid phase. The first KGT equation relates R_{tip} to the material properties, C_0 and Pe

$$R_{tip} = \sqrt{\frac{\Gamma D_\ell \left[1 - (1-k_p) Iv(Pe) \right]}{-mV(1-k_p)C_0}}; \qquad V = -\frac{mC_0(1-k_p)PeD_\ell}{k_p \left[1 - (1-k_p) Iv(Pe) \right] \Gamma}, \tag{10}$$

where $Iv(Pe)$ and Γ stand for the Ivantsov function and the Gibbs-Thompson coefficient, respectively. The second KGT equation relates ΔT to the material properties, C_0 and R_{tip}

$$\Delta T = m\left(C_0 - \frac{C_0}{1-(1-k_p)Iv(Pe)} \right) + \frac{2\Gamma}{R_{tip}}. \tag{11}$$

3 SOLUTION PROCEDURES

3.1 The distribution of the computational nodes

The computational nodes with typical Euclidian inter-nodal distances l_{macro} and l_{micro} are distributed at the macro and at the micro level, respectively, as shown in Figure 1. First, the temperature field at the computational points at the macro level is calculated, followed by the interpolation of the macroscopic temperature field to the computational points at the micro level, where the microscopic governing equations are solved.

3.2 Solution of the macroscopic model

At the macro level, the explicit Euler scheme is used for temporal discretization of the governing equation

$$\frac{\partial(\rho h)}{\partial t} \approx \frac{\rho h - \rho_0 h_0}{\Delta t_{macro}}, \tag{12}$$

where Δt_{macro} stands for the time step at the macro level. The LRBFCM is used for the spatial

discretization of the enthalpy equation. The computational nodes are grouped into overlapping local domains. A general quantity ϕ in the point $\boldsymbol{p}$ is approximated as

$$\phi(\mathbf{p}) \approx \sum_{k=1}^{{}_lK} {}_l\psi_k(\mathbf{p})\,{}_l\alpha_k, \tag{13}$$

where ${}_l\alpha_k$ and ${}_lK$ stand for the interpolation coefficients of the k-th node in the l-th local domain and the number of nodes in the l-th local domain, respectively. ${}_l\psi_k$ is the multiquadric radial basis function

$${}_l\psi_k(\mathbf{p}) = \sqrt{c\left(\frac{{}_lr_k}{l_{macro}}\right)^2 + 1}, \tag{14}$$

where ${}_lr_k$ and c stand for the distance between the point $\boldsymbol{p}$ and k-th node in the l-th local domain and the shape parameter, respectively. Shape parameter in each local domain is chosen according to the targeted condition number 10^{20} of the interpolation matrix.

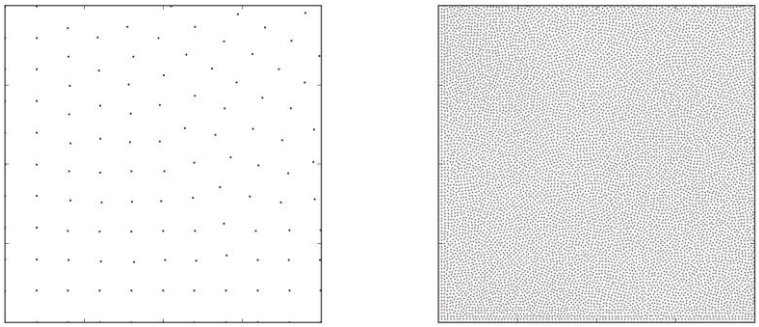

Figure 1: A section of the computational domain illustrating the distribution of the computational points at the macro (left) and at the micro (right) level.

3.3 Macro-micro interpolation

The temperature field is interpolated from the nodes at the macro level to the nodes at the micro level by using LRBFCM with multiquadric basis functions. The time step at the macro level Δt_{macro} is larger than time step at the micro level Δt_{micro}, hence a linear interpolation is used to determine the temperature in-between the interpolated temperatures T_i at two sequential macro times t^n_{macro} and t^{n+1}_{macro}

$$T(t) = T_i(t^n_{macro}) + \frac{T_i(t^{n+1}_{macro}) - T_i(t^n_{macro})}{\Delta t_{macro}}(t - t^n_{macro}); \qquad t^n_{macro} \le t \le t^{n+1}_{macro}. \tag{15}$$

3.4 Solution of the microscopic model - nucleation

At the micro level, the PA method is used to solve the nucleation and the grain growth equations. To each point (node) at the micro level an unsigned integer $\mathcal{S}$ is assigned. $\mathcal{S}$=0 represents the liquid phase and $\mathcal{S}$>0 the solid phase. Different non-zero values of $\mathcal{S}$ denote different grains. As the molten steel is poured into the mold, the whole system is in liquid

phase, hence $\mathcal{S}$=0 is assigned to each point in the computational domain at the beginning of the simulation. At every time step at the micro level, all the points with $\mathcal{S}$=0 are considered and different random numbers $r \in [0,1)$ are assigned to each of them. The nucleation at a point occurs, i.e., the point changes its $\mathcal{S}$ from $\mathcal{S}$=0 to $\mathcal{S}$>0, if [17]

$$r < V_{PA} \int_{\Delta T}^{\Delta T+\delta(\Delta T)} \frac{dn}{d(\Delta T')} d(\Delta T'), \tag{16}$$

where V_{PA} is the volume represented by the point and $\delta(\Delta T)$ is the change of the undercooling during one time-step. The assigned value $\mathcal{S}_r$ is a random non-zero unsigned integer calculated from r.

3.5 Solution of the microscopic model - growth velocity

The grain growth velocity as a function of undercooling is calculated by evaluating equations (10) and (11) for the equidistant values $\{Pe_1, Pe_2, ..., Pe_n\}$ with $Pe_1 = 4.0\,10^{-3}$, $Pe_n = 10.0$ and $n = 5000$. As the values $\{V(Pe_1), V(Pe_2), ..., V(Pe_n)\}$ and $\{\Delta T(Pe_1), \Delta T(Pe_2), ..., \Delta T(Pe_n)\}$ are calculated, least squares interpolation is performed to obtain

$$V(\Delta T) = a_1 \Delta T^3 + a_2 \Delta T^2 + a_3 \Delta T, \tag{17}$$

where $a_i, i = 1,2,3$ are the interpolation coefficients.

3.6 Solution of the microscopic model - grain growth

The PA method is also used for the solution of the grain growth equations. Each point with $\mathcal{S}$>0 has a neighbourhood defined with radius R as shown in Figure 2. Grain growth is represented as a growth of a circle with radius

$$l(t) = \int_{t_0}^{t} V(\Delta T) dt, \tag{18}$$

where t_0 is the time when the point was nucleated. Considering a solid point with $\mathcal{S}=\mathcal{S}_r>0$ and $l(t)<R$, the distances to its liquid neigbours are compared to $l(t)$. The liquid neighbouring point changes its index from $\mathcal{S}$=0 to $\mathcal{S}=\mathcal{S}_r$ if

$$l(t) \geq d, \tag{19}$$

where d is the distance between the solid and its neighbouring liquid point.

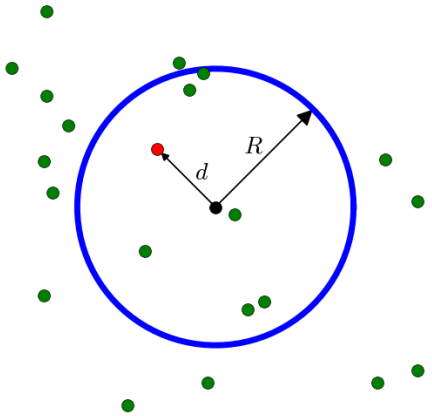

Figure 2: The neighbourhood of a point with $\mathcal{S} > 0$ defined by the radius R.

4 SIMULATION RESULTS

Simulation of the microstructure evolution is tested for the continuous casting of binary Fe-0.51wt%C steel. Square, H-profile and circular cross section geometries of the strand are used. For the heat transfer coefficient in equation (3), two different values are used

$$h_0 = \begin{cases} h_{mold}, & z < z_{mold} \\ h_{spray}, & \text{elsewhere} \end{cases}, \tag{20}$$

where h_{mold} and h_{spray} stand for the heat-transfer coefficients in the mold and in the spray section, respectively, and z_{mold} for the length of the mold. For the parameters of the normal distribution in equation (8) two different values are used

$$\Delta T_\sigma = \begin{cases} \Delta T_\sigma^{surface}, & d < d_{surface} \\ \Delta T_\sigma^{bulk}, & \text{elsewhere} \end{cases}, \quad \Delta T_\mu = \begin{cases} \Delta T_\mu^{surface}, & d < d_{surface} \\ \Delta T_\mu^{bulk}, & \text{elsewhere} \end{cases}, \tag{21}$$

where d and $d_{surface}$ stand for the distance between a computational node and the boundary and the thickness of the surface nucleation area, respectively. The final microstructures in the continuous casting of steel with square, H-profile and circular cross section geometry are shown in Figures 3, 4 and 5, respectively. The material properties, the continuous casting parameters and the numerical model parametes used are listed in Tables 1, 2 and 3, respectively. ECT and CET are observed in all three final microstructures.

Table 1: Material properties of the Fe0.51wt%C.

Property	Symbol	Unit	Value
Specific heat capacity in the liquid phase	c_ℓ	J/kg/K	1395.8
Specific heat capacity in the solid phase	c_s	J/kg/K	824.92
Thermal conductivity in the	k_ℓ	W/m/K	39.3

liquid phase			
Thermal conductivity in the solid phase	k_s	W/m/K	25.0
Density	ρ	kg/m^3	7430.0
Solute diffusion coefficient	D_ℓ	m^2/s	1.36 10^{-9}
Melting temperature of pure Fe	T_m	°C	1562.0
Partition coeffcient	k_p	-	0.37
Latent heat of fusion	h_f	J/kg	2.71 10^5
Liquidus line slope	m	°C/wt.%C	-30.0
Composition	C_0	wt.%C	0.51
Gibbs-Thompson coefficient	Γ	Km	1.9 10^{-7}

Table 2: Continuous casting parameters.

Parameter	Symbol	Unit	Value
Casting velocity	v_{cast}	m/min	1.0
Billet length	L_{billet}	m	25.0
Mould length	z_{mold}	m	0.8
Heat transfer coefficient in the mould area	h_{mold}	W/m^2/K	200.0
Heat transfer coefficient in the spray area	h_{spray}	W/m^2/K	80.0
Temperature of the cooling water	T_0	°C	30.0
Initial supercooling	ΔT_0	°C	25.0

Table 3: Numerical model parameters.

Parameter	Symbol	Unit	Value
Inter-nodal distance at the macro level	l_{macro}	m	2.0 10^{-3}
Inter-nodal distance at the micro level	l_{micro}	m	2.0 10^{-4}
Time step at the macro level	Δt_{macro}	s	1.0 10^{-2}
Time step at the micro level	Δt_{micro}	s	1.0 10^{-3}
Number of points in the collocation	${}_lK$	-	8
Thickness of the surface nucleation regime	$d_{surface}$	m	5.0 10^{-3}
Mean of the normal	$\Delta T_\mu^{surface}$	°C	0.6

distribution in the surface area			
Standard deviation of the normal distribution in the surface area	$\Delta T_{\sigma}^{surface}$	°C	0.2
Mean of the normal distribution in the bulk area	ΔT_{μ}^{bulk}	°C	7.0
Standard deviation of the normal distribution in the bulk area	ΔT_{σ}^{bulk}	°C	1.75
Neighbourhood radius in PA	R	m	$3.0\ 10^{-4}$
Growth velocity interpolation coefficient	a_1	$m/s/K^3$	$4.01\ 10^{-3}$
Growth velocity interpolation coefficient	a_2	$m/s/K^2$	$4.37\ 10^{-3}$
Growth velocity interpolation coefficient	a_3	m/s/K	$2.02\ 10^{-4}$

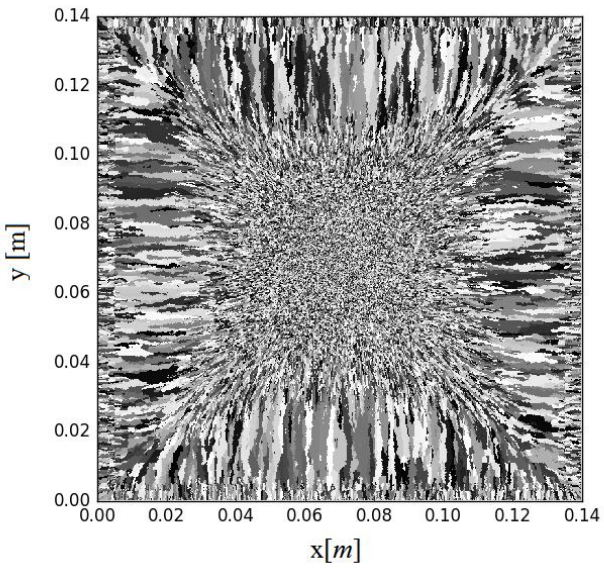

Figure 3: Final microstructure for the square cross section geometry of the strand.

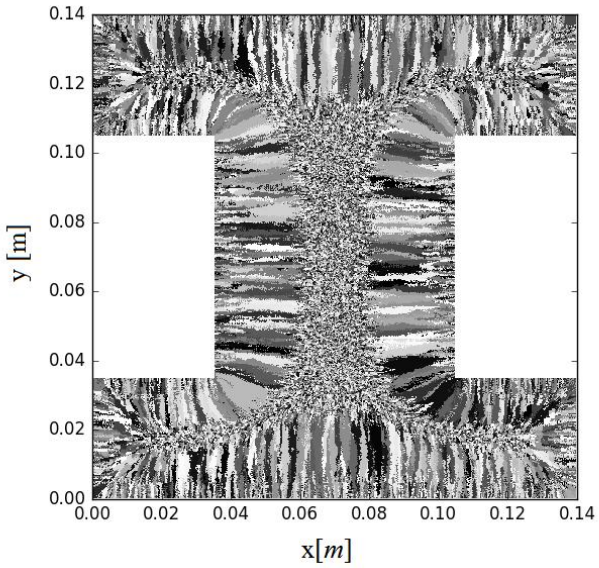

Figure 4: Final microstructure for the H-profile cross section geometry of the strand.

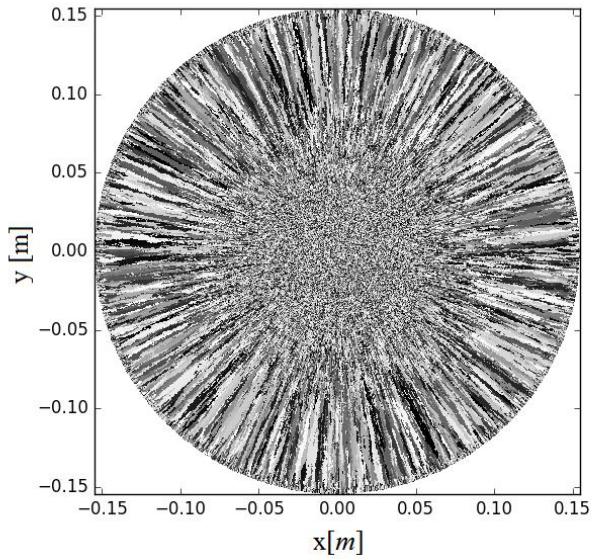

Figure 5: Final microstructure for the circular cross section geometry of the strand.

5 CONCLUSIONS

In the present paper, a two-scale slice model for simulation of microstructure evolution in the continuous casting of steel with arbitrary cross section geometry of the strand is presented. Meshfree LRBFCM and PA algorithms are used for the spatial discretization of the enthalpy equation and the solution of the microstructure evolution equations, respectively. The model

can be used for qualitative prediction of the microstructure evolution, e.g., for the determination of the ECT and CET positions in the continuous casting of steel. The material properties of the binary Fe-0.51wt%C steel that are used in the simulations can be replaced by material properites of multicomponent steels, obtained by JMatPro [18] database. Grain growth KGT equations become more complex in the case of multicomponent steels, since the concentrations and the partition coefficients of all alloyed elements have to be accounted for [19].

ACKNOWLEDGEMENTS

This work was funded by the Slovenian Grant Agency (ARRS) in the framework of applied research project L2-6775, co-sponsored by the companies IMPOL and Štore Steel.

REFERENCES

[1] Irving, W. R. *Continuous Casting of Steel*. Institute of Materials, (1993).
[2] Vertnik, R. and Šarler B. Solution of a continuous casting of steel benchmark test by a meshless method. *Eng. Anal. Bound. Elem.* (2014) **45**:45–61.
[3] Maurya, A. and Jha, P. K. Influence of electromagnetic stirrer position on fluid flow and solidification in continuous casting mold. *Appl. Math. Model.* (2017) In press, Corrected Proof.
[4] Dantzig, J. A. and Rappaz, M. *Solidification*. EFPL Press, (2009).
[5] Vušanović, I., Vertnik, R. and Šarler, B. A simple slice model for prediction of macrosegregation in continuously cast billets. *IOP Conf. Ser. Mater. Sci. Eng.* (2012) **27:**12056.
[6] Zhu, M. F. and Hong, C. P. A Modified Cellular Automaton Model for the Simulation of Dendritic Growth in Solidification of Alloys. *ISIJ Int.* (2011) **41**:436–445.
[7] Krane, M. J. M., Johnson, D. R. and Raghavan, S. The development of a cellular automaton-finite volume model for dendritic growth. *Appl. Math. Model.* (2009) **33**:2234–2247.
[8] Kobayashi, R. Modeling and numerical simulations of dendritic crystal growth. *Phys. Nonlinear Phenom.* (1993) **63**:410–423.
[9] Karma, A. and Rappel, W.-J. Quantitative phase-field modeling of dendritic growth in two and three dimensions. *Phys. Rev. E* (1998) **57**:4323.
[10] Boettinger, W. J., Warren, J. A., Beckermann, C. and Karma, A. Phase-Field Simulation of Solidification. *Annu. Rev. Mater. Res.*(2002) **32**:163–194.
[11] Gandin, C.-A. and Rappaz, M. A coupled finite element-cellular automaton model for the prediction of dendritic grain structures in solidification processes. *Acta Metall. Mater.*(1994) **42**:2233–2246.
[12] Lorbiecka, A. Z., Vertnik, R., Gjerkeš, H., Manojlovič, G., Senčič, B., Cesar, J. and Šarler, B. Numerical Modeling of Grain Structure in Continuous Casting of Steel. *Comput. Mater. Contin.* (2009) **8**:195–208.
[13] Lorbiecka, A. Z. and Šarler, B. Simulation of Dendritic Growth with Different Orientation by Using the Point Automata Method. *Comput. Mater. Contin.* (2010) **18**:69–104.
[14] Reuther, K. and Rettenmayr, M. Perspectives for cellular automata for the simulation of dendritic solidification–A review. *Comput. Mater. Sci.* (2014) **95**:213–220.
[15] Bennon, W. D. and Incropera, F. P. A continuum model for momentum, heat and species transport in binary solid-liquid phase change systems—I. Model formulation. *Int. J. Heat Mass Transf.* (1987) **30**:2161–2170.
[16] Kurz, W., Giovanola, B. and Trivedi R. Theory of microstructural development during rapid solidification. *Acta Metall.* (1986) **34**:823–830.
[17] Luo, S. and Zhu, M. Y. A two-dimensional model for the quantitative simulation of the dendritic growth with cellular automaton method. *Comput. Mater. Sci.* (2013) **71**:10–18.
[18] Saunders, N., Guo, U. K. Z., Li, X., Miodownik, A. P., Schilé, J. -Ph. Using JMatPro to model materials properties and behavior. *JOM* (2003) **55**:60–65.
[19] Šarler, B.,Vertnik, R., Lorbiecka, A. Z., Vušanović, I. and Senčič, B. A multiscale slice model for continuous casting of steel. *IOP Conf. Ser. Mater. Sci. Eng.* (2012) **33**:12021.